

# BIOCHEMICAL JOURNAL

## ACCEPTED MANUSCRIPT

Active site maturation and activity of the copper-radical oxidase GlxA is governed by a tryptophan residue

Amanda K. Chaplin, Dimitri A. Svistunenko, Michael A. Hough, Michael T. Wilson, Erik Vijgenboom and Jonathan A.R. Worrall

GlxA from *Streptomyces lividans* is a mononuclear copper-radical oxidase and a member of the auxiliary activity family 5 (AA5). Its domain organisation and low sequence homology make it a distinct member of the AA5 family in which the fungal galactose 6-oxidase (Gox) is the best-characterized. GlxA is a key cuproenzyme in the copper-dependent morphological development of *S. lividans* with a function that is linked to the processing of an extracytoplasmic glycan. The catalytic site in GlxA and Gox contain two distinct one-electron acceptors comprising the copper ion and a 3'-(S-cysteinyl) tyrosine. The latter is formed post-translationally through a covalent bond between a cysteine and a copper coordinating tyrosine ligand and houses a radical. In GlxA and Gox a second coordination sphere tryptophan residue (Trp288 in GlxA) is present, but the orientation of the indole ring differs between the two enzymes creating a marked difference in the  $\pi$ - $\pi$  stacking interaction of the benzyl ring with the 3'-(S-cysteinyl) tyrosine. Differences in the spectroscopic and enzymatic activity have been reported between GlxA and Gox with the indole orientation suggested as a reason. Here we report a series of *in vivo* and *in vitro* studies using the W288F and W288A variants of GlxA to assess the role of Trp288 on the morphology, maturation, spectroscopic and enzymatic properties. Our findings point towards a salient role for Trp288 in the kinetics of copper loading and maturation of GlxA, with its presence essential for stabilising the metalloradical site required for coupling catalytic activity and morphological development.

Cite as *Biochemical Journal* (2016) DOI: 10.1042/BCJ20160968

**Copyright 2016 The Author(s).**

Use of open access articles is permitted based on the terms of the specific Creative Commons Licence under which the article is published. Archiving of non-open access articles is permitted in accordance with the Archiving Policy of Portland Press (<http://www.portlandpresspublishing.com/content/open-access-policy#Archiving>).

Active site maturation and activity of the copper-radical oxidase GlxA is governed by a tryptophan residue

**Amanda K. Chaplin<sup>1</sup>, Dimitri A. Svistunenko<sup>1</sup>, Michael A. Hough<sup>1</sup>, Michael T. Wilson<sup>1</sup>, Erik Vijgenboom<sup>2</sup> and Jonathan A.R. Worrall<sup>1</sup>**

<sup>1</sup>School of Biological Sciences, University of Essex, Wivenhoe Park, Colchester, CO4 3SQ, U.K. <sup>2</sup>Molecular Biotechnology, Institute of Biology, Sylvius Laboratory, Leiden University, PO Box 9505, 2300RA Leiden, The Netherlands.

Running title: Trp288 regulates GlxA function

To whom correspondence should be addressed: Jonathan Worrall:

jworrall@essex.ac.uk: Tel. +44 1206 872095

**Key words:** Cuproenzyme, mononuclear copper-radical oxidase, *Streptomyces lividans*, post-translational modification, Cys-Tyr cross link

## ABSTRACT

GlxA from *Streptomyces lividans* is a mononuclear copper-radical oxidase and a member of the auxiliary activity family 5 (AA5). Its domain organisation and low sequence homology make it a distinct member of the AA5 family in which the fungal galactose 6-oxidase (Gox) is the best-characterized. GlxA is a key cuproenzyme in the copper-dependent morphological development of *S. lividans* with a function that is linked to the processing of an extracytoplasmic glycan. The catalytic site in GlxA and Gox contain two distinct one-electron acceptors comprising the copper ion and a 3'-(S-cysteinyl) tyrosine. The latter is formed post-translationally through a covalent bond between a cysteine and a copper coordinating tyrosine ligand and houses a radical. In GlxA and Gox a second coordination sphere tryptophan residue (Trp288 in GlxA) is present, but the orientation of the indole ring differs between the two enzymes creating a marked difference in the  $\pi$ - $\pi$  stacking interaction of the benzyl ring with the 3'-(S-cysteinyl) tyrosine. Differences in the spectroscopic and enzymatic activity have been reported between GlxA and Gox with the indole orientation suggested as a reason. Here we report a series of *in vivo* and *in vitro* studies using the W288F and W288A variants of GlxA to assess the role of Trp288 on the morphology, maturation, spectroscopic and enzymatic properties. Our findings point towards a salient role for Trp288 in the kinetics of copper loading and maturation of GlxA, with its presence essential for stabilising the metalloradical site required for coupling catalytic activity and morphological development.

## INTRODUCTION

GlxA from the Gram-positive soil dwelling bacteria *Streptomyces* is a structurally distinct member of the mononuclear copper-radical oxidase family [1]. Members contain a copper-radical active site in which the radical resides on a post-translationally formed 3'-(S-cysteinyl) tyrosine created through the covalent cross-linking of a Cys and Tyr residues [2-4]. This Cys-Tyr redox cofactor together with the one-electron acceptor copper (Cu) ion facilitates the two-electron stereospecific oxidation of a range of primary alcohols to the corresponding aldehyde, with the concomitant production of H<sub>2</sub>O<sub>2</sub> as a result of reduction of the co-substrate oxygen [5, 6]. In the CAZy (Carbohydrate Active enZyme) database, mononuclear Cu-radical oxidases are classed into the auxiliary activity family 5 (AA5) [7, 8]. Phylogenetically, the AA5 family can be divided into two sub-families; subfamily 1 includes known (methyl)glyoxal oxidases and subfamily 2 encompasses galactose 6-oxidases [9]. GlxA however, is not associated with either subfamily.

The *glxA* gene is widespread in actinobacteria, where recent studies have brought to the foreground the central role GlxA has in the Cu-dependent morphological development of the biotechnology important strain *Streptomyces lividans*. GlxA is transcriptionally coupled to CslA, which belongs to the GlycosylTransferase Family 2, and includes cellulose and chitin synthases, amongst others [7]. Together CslA and GlxA produce/modify a  $\beta$ -(1,4)-glycan, of unknown chemical composition. This glycan has been demonstrated to be critical for development of aerial hyphae as the microbe switches from vegetative to aerial growth coupled with the secretion of secondary metabolites such as antibiotics [1, 10, 11]. Deletion of *csIA* blocks the formation of reproductive aerial hyphae on solid medium [10, 11]. Likewise, a *glxA* null mutant blocks development, coinciding with the loss of glycan deposition at hyphal tips; the same phenotype as observed with the *csIA* deletion [1, 12]. This is consistent with a model whereby CslA and GlxA cooperatively function in glycan deposition at the hyphal tip and are jointly responsible for the formation of reproductive aerial structures [1].

Galactose 6-oxidase (Gox) from *Fusarium graminearum* is the best studied AA5 subfamily 2 member [6]. Its tertiary structure consists of three domains, with domain 2 housing the Cu active site close to the solvent surface (Fig. 1A). The Cu ion is coordinated equatorially by the N $\epsilon$  atoms of two His residues, the O $\gamma$  atom of the

3'-(S-cysteinyl) tyrosine and a H<sub>2</sub>O molecule, with axial ligation provided by the O $\gamma$  atom of a Tyr residue, completing a square pyramidal coordination geometry (Fig. 1B). GlxA has an identical first sphere Cu coordination (Fig. 1B) and a tertiary structure comprising of three domains (Fig. 1A). However, the domain arrangement is distinctly different between GlxA and Gox (Fig. 1A), with the Cu site in GlxA occluded from solvent, in part from the positioning of domain 2 on top of domain 1 and is only accessible through tunnels leading down from entrances at specific surface sites [1]. Despite the high similarity in Cu coordination between Gox and GlxA, catalytically GlxA displays only residual activity with substrates that are readily turned over by Gox [1]. The only *in vitro* substrate discovered to date that GlxA has significant activity for is glycolaldehyde (HC(O)-CH<sub>2</sub>OH), a diose which may be considered as the simplest sugar-like molecule [1].

Spectroscopically GlxA also differs to Gox [1]. The UV-vis absorbance spectra of semi-reduced, Cu(II)-(Cys-Tyr), and fully oxidised Cu(II)-(Cys-Tyr $\bullet$ ), states are very different compared to the corresponding oxidation states in Gox [1]. A second coordination sphere Trp residue in Gox (Trp290), referred to as the 'stacking' Trp owing to the benzene moiety of the indole ring stacking over the Cys<sup>228</sup>-S $\gamma$ -C $\epsilon$ -Tyr<sup>272</sup> bond of the 3'-(S-cysteinyl) tyrosine has received particular attention [3]. This Trp residue (Fig. 1B) has been shown to have implications on the catalytic activity of Gox and on radical stabilisation and is an exemplar of how a second sphere coordinating residue can influence the properties of a metalloenzyme [13, 14]. A 'stacking' Trp residue in GlxA (Trp288) is also present (Fig.1B), but the stacking orientation of the indole ring is distinctly different from that of Trp290 in Gox. In GlxA, Trp288 is the adjacent residue to Tyr289, which forms the 3'-(S-cysteinyl) tyrosine residue, but in Gox, Trp290 is located on a separate loop structure. The indole ring orientation of Trp288 in GlxA is such that the benzyl ring is  $\pi$ - $\pi$  stacking with the phenolate of the 3'-(S-cysteinyl) tyrosine leaving the Cys<sup>121</sup>-S $\gamma$ -C $\epsilon$ -Tyr<sup>289</sup> bond of the 3'-(S-cysteinyl) tyrosine exposed. This contrasts with Gox where the benzyl group of Trp290 lies directly over the Cys-Tyr bond and the pyrrole group lies over the Tyr of the 3'-(S-cysteinyl) tyrosine (Fig. 1B) [3].

In the present work, we have addressed the role of Trp288 on the functional and structural properties of GlxA. We find that this second sphere coordination residue influences the processing of premature GlxA to the mature form (*i.e.* Cu-

loaded and the 3'-(S-cysteinyl) tyrosine formed). Furthermore, its absence leads to the electronic absorption spectrum having properties that resemble Gox, with the evolution of the absorbance spectrum following addition of Cu(II) ions to the premature form kinetically dependent on the type of substitution made at the 288 position. Finally, we show that the absence of Trp288 severely retards the formation of the radical on the Cys-Tyr cross-link with implications for catalytic activity *in vitro* and *in vivo* as well as on the morphological development of *S. lividans*.

## EXPERIMENTAL PROCEDURES

### *Complementation plasmids*

Construction of the *glxA* null mutant in the *S. lividans* 1326 strain is described in [1]. Plasmids for the complementation of the *glxA* null mutant consisted of pSET152 backbone with the *glxA* ORF under control of the *csIA* promoter (-545 to -1 upstream of *csIA*, *SLI\_3187*), pGLXA (wild-type), pGLXA-W288A and pGLXA-W288F. Following protoplast transformation these plasmids integrate in the genome at the phage  $\Phi$ C31 attachment site. The *csIA* promoter fragment and the fragment harbouring the *glxA* ORF were obtained by PCR with primers (the relevant restriction sites introduced in the primers are in bold or double underlined). For the *csIA* promoter region the primers used were: GCGGAATTCCTCACACTCCCGGTCGGCAGG (P2836F) and CGCGGATCCATATGTCATTCCCCCACACGCGGGTC (P2836R); for the *glxA* ORF the primers used were: GCG GAA TTC CAT ATG AAA GAC CGT GCC GGC CGC (2837F) and CGCGGATCCGGCGCTACGGAACTCGCACC (2837R). The *glxA* mutations were introduced in the complementation plasmid by restriction digest and ligation making use of a unique BtsI restriction site in position +222 relative to the *glxA* start codon. The vector pSET152 was digested with EcoRI and BamHI, the *csIA* promoter and the first 224 nt of the *glxA* ORF were isolated as a EcoRI-BtsI fragment from pGLXA harbouring the *csIA* promoter and wild-type *glxA* ORF on a EcoRI-BamHI fragment. The fragments harbouring the mutation were isolated from the respective pET28a-*glxA* plasmids (*vide infra*) as BtsI-BamHI fragments. Following three fragment ligations and transformation to competent *Escherichia coli* JM109 cells, plasmids isolated from two transformants of each were sequenced to confirm the presence of the mutation in the *glxA* ORF. For

complementation studies these plasmids were introduced in the *S. lividans*  $\Delta$ *glxA* mutant strain by protoplast transformation.

#### *Growth morphology of S. lividans*

For surface growth the agar media R5 [15] with 5  $\mu$ M Cu(II)SO<sub>4</sub> added was used and incubated at 30 °C. Spore stocks were diluted to 3x 10<sup>4</sup>/mL and 20  $\mu$ L was spotted on the R5 agar. Digital images of the plates were taken after 6 days incubation and individual spots were cropped without further digital manipulation. Morphology in liquid media was determined following 18 h growth at 30 °C with shaking in baffled flasks containing Tryptic Soya Broth (TSB) supplemented with 10 % sucrose and 5  $\mu$ M Cu(II)SO<sub>4</sub>. Cultures were inoculated with freshly isolated spores at 2x 10<sup>6</sup>/mL. Samples from liquid cultures were analysed by light microscopy with a Zeiss Standard 25 microscope and digital images were taken with AxioCam linked to AxioVision software. All spore stocks were obtained from cultures grown on soya flour mannitol agar plates with 50  $\mu$ g/mL apramycin to select for the integrated pSET152 plasmid, resuspended in 30 % glycerol and stored at -20 °C.

#### *Construction of the GlxA W288A and W288F variants*

Quikchange mutagenesis was used to produce the GlxA W288A and W288F variants. Forward and reverse primers (25 bps) containing the desired nucleotide changes were synthesized (Sigma) and a PCR reaction mix consisting of 75 ng/ $\mu$ l of the respective mutagenic primers, 15 ng/ $\mu$ l of template DNA [1], Pfu Turbo polymerase (Stratagene), Pfu buffer (Stratagene), dNTP's (ThermoFisher) and DMSO (Sigma) prepared to a final volume of 30  $\mu$ l. The PCR product was subjected to a DpnI digestion and transformed into *Escherichia coli* JM109. All clones were DNA sequenced.

#### *Over-expression and purification of wild-type and GlxA variants*

Wild-type (WT) GlxA (residues 35-645) and GlxA variants used in this work (C121G, W288A and W288F) were over-expressed in *E. coli* BL21(DE3) cells. To produce wild-type (WT) apo-GlxA an auto-induction media [16] and growth conditions was necessary as previously described [17]. Details of the over-expression and purification protocols are given in Supplementary Information.

### *GlxA sample preparation*

All protein samples were exchanged into the desired buffer using PD-10 desalting columns (GE-Healthcare) and concentrated using 30 kDa cut-off centricons (Satorius). Cu(II)-loaded samples were prepared by the addition of a stoichiometric equivalent or excess of a stock Cu(II)SO<sub>4</sub> (Sigma) solution. The oxidants K<sub>3</sub>[Fe(CN)<sub>6</sub>] (Sigma) or K<sub>2</sub>[Ir(Cl)<sub>6</sub>] (Acros) were added to Cu(II)-loaded samples in > 5-fold excess and removed using a PD-10 column. GlxA concentrations were determined spectrophotometrically using extinction coefficient ( $\epsilon$ ) at 280 nm determined using the ExPASy server of 78,730 M<sup>-1</sup> cm<sup>-1</sup> for WT and the C121G variant and an  $\epsilon_{280}$  of 73,320 M<sup>-1</sup> cm<sup>-1</sup> for the W288A and W288F variants [18]. UV-visible absorption spectra were measured on a Varian Cary 60 spectrophotometer at 20 °C.

### *Electron paramagnetic resonance (EPR) spectroscopy and spectral simulations*

EPR samples were prepared in a mixed buffer system consisting of 10 mM Tris, potassium acetate, MES, MOPS and 200 mM KCl, pH 7. Samples (120  $\mu$ M) were placed in Wilmad SQ EPR tubes to a final volume of 250  $\mu$ l, frozen in methanol kept on dry ice, wiped and then transferred to liquid nitrogen. EPR spectra were measured at 40 K on a Bruker EMX EPR spectrometer (X-band) at a modulation frequency of 100 kHz. A spherical high-quality Bruker resonator ER 4122 SP9703 and an Oxford instruments liquid helium system were used to measure the low temperature EPR spectra. The EPR spectra of the blank samples (frozen water) were subtracted from the EPR spectra of the protein samples to eliminate the baseline caused by the resonator walls, quartz insert or EPR tube. Residual baselines were corrected using WinEPR v. 2.22 (Bruker Analytik, GmbH) by subtraction of a polynomial line drawn through a set of points randomly chosen on the baseline. Spectral simulations were carried out using SimFonia v. 1.26 (Bruker Analytik, GmbH). The  $g_z$  component and its hyperfine splitting constant  $A_z^{\text{Cu}}$  were determined directly from the spectra. Rather than varying  $g_x$  and  $g_y$  independently, two other values,  $g_{\text{av}}$  and  $\Delta g$ , were varied, where  $g_{\text{av}} = (g_x + g_y)/2$  and  $\Delta g = g_y - g_{\text{av}} = g_{\text{av}} - g_x$ . To maintain consistency in the simulation procedure while varying the minimal number of parameters, several constraints were imposed on the choice of the other simulation parameters thus



minimising the number of varied parameters. Thus, the tensor for the hyperfine interaction of the spin density with Cu nucleus  $A^{\text{Cu}}$  ( $I_{\text{Cu}} = 3/2$ ) was assumed axial, with the  $A_x^{\text{Cu}} = A_y^{\text{Cu}} = 0.1 A_z^{\text{Cu}}$  (small variations around empirically picked factor of 0.1 were found to produce minimal effect on the simulated spectra). Furthermore, all  $A^{\text{Cu}}$  tensors were assumed collinear with the g-tensor (all Euler angles were assumed zero). Cu coordinating nitrogen atoms ( $I_{\text{N}} = 1$ ) were assumed to produce isotropic hyperfine interactions ( $A_x^{\text{N}} = A_y^{\text{N}} = A_z^{\text{N}} = 14 \text{ G}$ ). In accordance with earlier reported relationship between principal g-factor components and individual line width values along those directions [19], the x-, y- and z- components of the spectra line width  $\Delta H$  were assumed to have similar dependences – almost linear with gradually changing moderate slopes - the higher the  $g_i$ , the higher the  $\Delta H_i$  value. These dependences were maintained for all simulations. Thus, the constraints imposed on the simulation process allowed the best fits by varying just two numbers,  $g_{\text{av}}$  and  $\Delta g$ , while  $g_z$  and  $A_z^{\text{Cu}}$  were found directly from experimental spectra.

#### *Stopped-flow kinetics*

A SX20 stopped-flow spectrophotometer (Applied Photophysics) equipped with a diode array multi-wavelength unit or single wavelength photomultiplier, thermostatted at 25 °C was used. GlxA samples (17  $\mu\text{M}$  after mixing) were prepared in 50 mM Tris/HCl pH 8, 150 mM NaCl and rapidly mixed with excess  $\text{Cu(II)SO}_4$  solutions (40 to 600  $\mu\text{M}$  after mixing). Spectra were recorded using the diode array multi-wavelength unit to observe all spectral transitions, with reactions then monitored using single wavelengths at 280 nm and 480 nm. All data were analysed using the Applied Photophysics ProKineticist software. Rate constants were obtained by fitting the data at 280 nm and 480 nm to single exponential functions and plotted as a function of  $[\text{Cu(II)}]$ .

#### *Activity assays*

Enzymatic activity using glycolaldehyde (Sigma) was monitored through a coupled peroxidase assay as described previously [1]. In brief,  $\text{H}_2\text{O}_2$  production was detected by the presence of horseradish peroxidase (HRP) (Sigma) and the subsequent oxidation of guaiacol (Sigma). Samples were prepared in 3 ml cuvettes containing 0.1 M sodium phosphate pH 7.4, 1 mM guaiacol, 1  $\mu\text{l}$  HRP (10  $\text{mg ml}^{-1}$ ), 20-30  $\mu\text{M}$  of

GlxA or variant and glycolaldehyde (5 to 300 mM). Guaiacol oxidation was monitored at 470 nm using a Hewlett-Packard 8453 diode-array spectrophotometer scanning between 190 and 1100 nm and thermostatted at 25 °C.

#### *Western blotting*

GlxA samples incubated with Cu(II) ions were quenched at known time periods by the addition of SDS-PAGE buffer, followed by heating at 95 °C and snap freezing (-80 °C). Western blotting was carried out by loading samples (~ 5 ng) to a 7.5 % SDS-PAGE gel (BioRad) followed by transfer to polyvinylidene difluoride (PVDF) membranes (BioRad) and then incubated overnight at 4 °C with GlxA polyclonal antibodies (1:20,000) [17]. The PVDF membranes were then washed and incubated at room temperature with goat anti-rabbit alkaline phosphatase, with detection carried out with NBT/BCIP (Nitro blue tetrazolium/bromo-4-chloro-3-indolyl phosphate (Sigma).

#### *Crystallisation and X-ray structure determination of the GlxA W288A variant*

An ARI-Gryphon crystallisation robot was used to screen crystallisation conditions. Crystal hits in the PEG suite (Qiagen) screen were obtained for the as isolated W288A variant. Scaling-up and optimisation from the initial hit was carried out in 24-well VDX plates (Molecular Dimensions) using the hanging drop vapor diffusion method at 18 °C. Equal volumes of protein (15 mg ml<sup>-1</sup>) and reservoir solution (20 % w/v 20 K polyethylene glycol, 0.1 M sodium acetate, pH 4) were mixed and long needle like crystals suitable for diffraction studies grew within 48 h. Single crystals were transferred to a cryoprotectant solution containing the respective reservoir solution and 20 % ethylene glycol prior to flash-cooling by plunging into liquid nitrogen. Cu(II)-soaking of W288A crystals was carried out by the addition of 10 mM Cu(II)SO<sub>4</sub> to the cryoprotectant solution and crystals left to soak for various times before cooling in liquid nitrogen. Crystallographic data were measured at beamline I03, Diamond Light Source, using an X-ray wavelength of 1.00 Å and a Pilatus 6 M-F detector (Dectris). Data were processed automatically using XDS [20] in XIA2 [21] and scaled and merged using Aimless [22] in the CCP4i suite. Structures were solved by molecular replacement using Molrep with the WT GlxA structure (4nm) as the search model [1]. Structures were refined using Refmac5 [23], with model building between refinement cycles in Coot [24]. Riding hydrogen atoms were added when

refinement of the protein atoms had converged. Structures were validated using the Molprobity server [25], the JCSG Quality Control Server and tools within Coot [24]. Structural superpositions were carried out using GESAMT in CCP4i2 [26]. Coordinates and structure factors were deposited in the RCSB Protein Data Bank. A summary of data, refinement statistics and the quality indicators for the structures are given in Table 1.

## RESULTS

### *The GlxA W288A and W288F variants are over-expressed and purified in a premature form*

Heterologous expression of the W288A and W288F variants yielded purified samples conspicuous by the absence of the blue-grey colour associated with wild-type (WT) GlxA produced under the same conditions. UV-vis spectroscopy did not give the expected transitions in the visible region associated with the Cu(II)-(Cys-Tyr) form of GlxA, suggesting both variants were produced in the apo-form (Fig. S1). Immunoblot analysis revealed that both the W288A and W288F variants migrated at the same height (molecular weight) on a SDS-PAGE gel relative to the C121G GlxA variant (Fig. 2A and B) [17], which is incapable of forming the 3'-(S-cysteinyl) tyrosine amino acid. Previous reports with Gox and GlxA [13, 17], have revealed that the presence of the 3'-(S-cysteinyl) tyrosine (mature GlxA) results in a more rapid migration on the gel as the Cys-S $\gamma$ -C $\epsilon$ -Tyr bond prevents complete linearization (Fig. 2A and B). Therefore, as isolated and purified the W288A and W288F variants are consistent with a premature form where the 3'-(S-cysteinyl) tyrosine is not formed.

### *Trp288 influences Cu uptake and maturation*

Incubation of the W288A and W288F variants with stoichiometric quantities of Cu(II) ions in aerated buffer resulted in the clear detection of two bands by immunoblot analysis, with migration patterns consistent with the presence (lower band) and absence (upper band) of the 3'-(S-cysteinyl) tyrosine amino acid. Band intensities throughout the time range in which samples were incubated with Cu reveal an approximately equal distribution of the mature and premature forms (Fig. 2A and B). It is noted in Fig. 2B that some intensity at the position expected for the mature GlxA is present for apo-W288F. This could be due to some degradation in the samples since

more, faster migrating low intensity bands are present in several lanes of this blot. Regardless of this the interpretation that incomplete processing occurs with equal proportions of premature and mature GlxA still holds for the two variants. Further additions of Cu to the W288A and W288F variants did not lead to the presence of a single mature band. To assess whether incomplete processing was due to the absence of Trp288, WT GlxA was produced and purified in the apo-form. Immunoblot analysis revealed that only the upper band was present, consistent with the absence of the 3'-(S-cysteinyl) tyrosine (Fig. 2C). Following aerobic incubation with Cu(II) ions, two bands were again detected. In contrast to the W288A and W288F variants the formation of the 3'-(S-cysteinyl) tyrosine continued after 1 h incubation, with ~ 75% of mature GlxA present after 72 h (Fig. 2C). As with the W288A and W288F variants, addition of excess Cu did not lead to the formation of a single band. Thus, Trp288 affects Cu uptake during heterologous over-expression in *E. coli* of GlxA and influences the extent to which the fully matured form is processed *in vitro*.

#### *The Trp288 variants significantly alter the Cu electronic absorption spectrum*

The stoichiometric addition of Cu(II) ions to the W288A and W288F variants was monitored by UV-vis spectroscopy. For both variants, the concomitant appearance of absorbance bands at  $\lambda_{\max}$  479 nm (W288F) and 477 nm (W288A) and a broad low intensity absorbance band at  $\lambda_{\max}$  750 nm was observed (Fig. 3A and B). For the W288F variant the absorption bands appeared rapidly following Cu(II) addition and did not change in intensity or wavelength upon further Cu(II) additions. This behaviour allowed the stoichiometry of Cu(II)/enzyme to be determined through Cu(II) ion additions titrated to the apo-enzyme to reveal a linear relationship between  $\Delta$ Abs and [Cu(II)] until a break point at a stoichiometry of ~ 1:1 was reached. This is indicative of a high affinity Cu(II) binding process (inset Fig. 3A). For the W288A variant evolution of the two absorption bands upon addition of a stoichiometric equivalent of Cu(II) was considerably slower compared to the W288F variant, with a rate constant for the formation of the 480 nm band of  $k = 2.2 (\pm 0.06) \times 10^{-3} \text{ min}^{-1}$  (inset Fig. 3B). No further absorbance increases on subsequent additions of Cu(II) ions were observed, again consistent with a stoichiometry for Cu binding of 1:1 for this variant. Furthermore, the absorbance spectra of the W288A and W288F variants once Cu-loaded did not change over prolonged periods of time (> 72 h). However, it

is noted that the W288A and W288F variant spectra differ significantly from that of the WT Cu(II)-(Cys-Tyr) spectrum (Fig. 3C), where a broad absorbance band at  $\lambda_{\max}$  577 nm and shoulders at 362 and 320 nm are observed (Fig. 3C). The addition of the oxidants  $K_3[Fe(CN)_6]$  ( $E^0 = +436$  mV vs SHE) or  $K_2[IrCl_6]$  ( $E^0 = +710$  mV vs SHE) did not perturb the absorbance spectra for the W288F and W288A variants, and is also the case for WT GlxA [1] (data not shown).

*The size of the residue at position 288 in GlxA affects the X-band EPR parameters*

EPR spectra for WT and the W288A and W288F GlxA variants in the Cu(II)-(Cys-Tyr) state are reported in Fig. 4A. To understand the structural distinctions that underlie the differences in the EPR line shapes, we simulated the Cu(II) EPR spectra. Attempts to simulate these spectra as a single Cu(II) species proved unsuccessful. However, simulation was possible if a linear combination of two different line-shapes was assumed (Fig. 4A), each using a  $CuN_2$  spin system but with differing simulation parameters as specified in Table 2. Thus, each experimental EPR spectrum is best approximated by a superposition of two different EPR line types, further referred to as Sim1 and Sim2, from two different Cu(II) complex types. The experimentally determined  $A_z$  and  $g_z$  values for Sim1 for WT GlxA place the Cu(II) site within the Type 2 definition of Peisach and Blumberg [27]. A notable difference between the line shapes of Sim1 and Sim2 is the presence of a strong ‘overshoot’ line in Sim2 just above 3,400 G (Fig. 4A). This feature is a consequence of a special geometry of Cu(II) coordinating ligands, a combination of two factors that are different in Sim2 as compared to Sim1: a smaller  $g$ -factor anisotropy (resulting in a smaller  $g_z$  value) and a larger  $A_z$  value (Table 2). Importantly, although Cu(II) EPR spectra are typically nearly axial ( $g_y \approx g_z$ ), none of the six considered Cu(II) EPR signals can be simulated for an axial coordination of the metal centre, thus a rhombic distortion ( $g_x \neq g_y \neq g_z$ ) to the overall geometry of the ligand field is obtained (Table 2). As the side chain of the residue replacing Trp288 becomes smaller (Trp to Phe to Ala), the weight of the ‘overshoot’ type Cu(II) complex Sim2 decreases dramatically from 61 % to 47 % to 27 %, respectively. Also, several trends in the parameters of the two Cu(II) complexes become apparent (Fig. 4B). For instance, the  $g_z$  value of Sim1 becomes higher – increasing from 2.270 to 2.283 ( $\Delta 0.013$ ) while  $g_z$  of Sim2 becomes smaller – decreasing from 2.182 to 2.178 ( $\Delta 0.004$ ) (Fig. 4B). Furthermore,  $A_z^{Cu}$  of Sim1

drastically decreases from 172 G in WT to 155 G in W288F and to 137 G in W288A, while  $A_z^{\text{Cu}}$  of Sim2 exhibits more moderate changes in the opposite direction – the value increases from 202 G (WT and W288F) to 215 G (W288A) (Fig. 4B). Therefore, in accord with the perturbation of the electronic absorption spectrum of the W288A and W288F variants Trp288 is also contributing to the EPR spectral parameters.

#### *Stopped-flow kinetics reveals a fast-initial Cu(II) binding phase in GlxA*

To explore further the mechanism of Cu(II) loading and binding stopped-flow kinetic experiments were carried out. The W288A and W288F variants were mixed with excess Cu(II) solutions and changes in absorbance were monitored at 480 nm, to correspond with the observation from static experiments (Fig. 3A and B). As expected only the W288F variant displayed an absorbance change at 480 nm under time-scales employed in the stopped-flow experiment (inset Fig. 5A). The kinetic traces were fitted to a single exponential function yielding pseudo-first order rate constants ( $k_{\text{obs}}$ ), plotted against [Cu(II)] to reveal a non-linear concentration dependence (Fig. 5A). Closer inspection of the kinetic traces revealed a lag within the first 5-10 s (inset Fig. 5A), suggesting that the transition observed at 480 nm is not the initial binding event. This is further supported by the non-linear [Cu(II)] dependence of the pseudo-first order rate constant (Fig. 5A). Upon monitoring other wavelengths, a fast phase could be detected at 280 nm, with a time course (5-10 s) corresponding to the lag identified at 480 nm (inset Fig. 5B). The kinetic traces could be fitted to a single exponential function to give  $k_{\text{obs}}$  that followed a linear dependence on [Cu(II)] (Fig. 5B), enabling a second-order rate constant ( $k_1 = 2.2 \pm 0.2 \times 10^3 \text{ M}^{-1}\text{s}^{-1}$ ) for Cu(II) binding to be determined. This initial Cu(II) binding phase identified for the W288F variant at 280 nm was also observed for the W288A variant upon mixing with excess Cu(II) solutions (inset Fig. 5C). The kinetic traces were fitted to a single exponential function to again reveal a linear dependence of  $k_{\text{obs}}$  on [Cu(II)] (Fig. 5C), with a second order rate constant of  $k_1 = 2.8 \pm 0.06 \times 10^3 \text{ M}^{-1}\text{s}^{-1}$ .

These kinetic data suggest a sequential mechanism for binding Cu(II), which can be described by **Scheme 1**. An initial rapid weak interaction is observed at 280 nm for both the W288F and W288A variants to form GlxA\*Cu(II), followed by a slow step (observed at 480 nm) to give the final GlxA-Cu(II) complex. The slow step may be considered as a rearrangement step leading to the formation of a Cu(II) site

with a very high binding affinity. No rate constant is assigned to the dissociation of Cu(II) from Cu(II)-GlxA because titrating Cu(II) into the W288F variant suggests an equilibrium dissociation constant ( $K_d$ ) with an upper limit of  $10^{-8}$  M (inset Fig. 3A), and thus the dissociation rate constant would be very small. The first step is much faster than the second and may be considered in an equilibrium throughout all times of the reaction. This yields a slight [Cu(II)] dependence of the slow step (Fig. 5A), whereby the  $k_{\text{obs}}$  may be described by Equation 1,

$$k_{\text{obs}} = \frac{k_2[\text{Cu(II)}]}{K_d + [\text{Cu(II)}]} \quad (1)$$

and used to fit the data in Fig. 5A to yield a first-order rate constant ( $k_2 = 0.041 \pm 0.01$  s<sup>-1</sup>) for the slow rearrangement phase at 480 nm and a  $K_d$  of  $36 \pm 3$   $\mu$ M for the initial Cu(II) binding (GlxA\*Cu(II)) for W288F. This enables a dissociation rate constant ( $k_1 = 0.08 \pm 0.01$  s<sup>-1</sup>) to be calculated with a value somewhat larger than the intercept of  $k_{\text{obs}}$  for the fast phase (Fig. 5B), but still in reasonable agreement.

#### *Structural changes accompanied by Cu(II)-loading to GlxA*

The X-ray crystal structure of the as purified W288A GlxA variant was determined to 1.92 Å resolution, with two molecules in the crystallographic asymmetric unit (Table 1). The mutation has minimal impact on the overall tertiary structure (a C $\alpha$  superposition with WT GlxA gave a RMSD value of 0.31 Å). Inspection of the active site revealed no electron density that could be assigned to a Cu ion, thus the structure determined is that of the apo-form (Fig. 6A), confirming initial interpretation from UV-vis spectroscopy. The spatial arrangement of the axial Tyr501 ligand and the two equatorial His ligands are relatively well conserved between the apo-W288A and the holo-WT structures (Fig. 6B). However, the 3'-(S-cysteiny) tyrosine is not formed resulting in structural rearrangement of the Cys121 and Tyr289 side chains (Fig. 6A). The plane of the Tyr289 phenol ring is rotated by  $\sim 90^\circ$  relative to WT enabling for a H-bond interaction with a H<sub>2</sub>O molecule, and the Cys121 side chain is rotated around  $\chi_1$  so that the thiol group is now pointing away from the plane of the phenol ring (Fig. 6A and B). This new conformation of Tyr289 would not be possible in WT GlxA as it would be sterically hindered by the indole ring of Trp288 (Fig. 6B).

Structural changes associated with Cu binding were determined through aerobic soaking of the W288A crystals with excess Cu(II) ions. Various soak times were experimented with, ranging from a few min to > 1 h. The diffraction quality of the soaked crystals was found to be highly dependent upon soaking times, with the best diffracting crystals found after ~ 10 min. A 1.49 Å resolution structure of a Cu(II)-soaked crystal with one protein molecule in the crystallographic asymmetric unit was determined (Table 1). A C $\alpha$  superposition of this structure with WT and apo-W288A GlxA gave RMSD values of 0.57 Å and 0.66 Å, respectively. A strong positive 22  $\sigma$ -peak in the  $\sigma$ A-weighted F<sub>o</sub>-F<sub>c</sub> difference map was observed, into which a Cu ion was modelled with an occupancy of 0.7 (Fig. 6C). Notably, electron density for the side-chains of Phe261, Tyr289 and Cys121 is consistent with the existence of two alternate conformations (Fig. 6C). The major conformation (occupancy 0.7) is associated with the Cu-coordinated fraction and is closer to the holo-GlxA active site structure (Fig. 6B). In both conformations, Cys121 is oriented towards the Cu and Tyr289 but more distant from both than in holo-GlxA (Fig. 6B). In the major conformation, the Cys121-S $\gamma$  to Tyr289-C $\epsilon$ 1 distance is 3.7 Å, suggesting that the 3'-(S-cysteinyl) tyrosine is not formed, although the side chains are oriented favourably for such a cross-link to form. The minor conformation (occupancy 0.3), with the Tyr289 ring plane rotated ~ 90° away from its position in the major occupancy state (and holo-GlxA) is more reminiscent of the apo-W288A structure and does not enable for a coordinate bond between the Cu and the O $\gamma$  of Tyr289. The distance between the O $\gamma$  of the Tyr501 and the Cu ion is 2.8 Å, elongated from the ~ 2.2 Å bond present in holo-GlxA [1]. Overall, these structural observations lend support to the immunoblot analysis (Fig. 2), that the *in vitro* addition of Cu(II) drives the formation of the 3'-(S-cysteinyl) tyrosine, but not to completion.

Residue Phe261 is part of a putative substrate tunnel (tunnel I) previously identified in WT GlxA [1]. By substituting Trp288 for an Ala, Phe261 gains conformational flexibility due to the absence of steric restraints imposed by Trp288. In apo-W288A, Phe261 occupies a conformation like that in WT (Fig. 6B), which allows space for Tyr289 to flip away from the Cu site (*vide supra*). In Cu-W288A, two conformations are present, one like WT and apo-W288A, while in the second, Phe261



has flipped into a spatial position that is only sterically feasible due to the absence of Trp288 and the rotation of Tyr289 into a Cu-coordinating position (Fig. 6B).

#### *The W288A and W288F variants do not turnover glycolaldehyde*

The physiological substrate for GlxA is presently undetermined. Unlike Gox, which has a broad substrate specificity *in vitro* [5], the diose glycolaldehyde is the only known compound to have activity with GlxA [1]. However, the catalytic efficiency at pH 7.4 is low with a  $k_{\text{cat}}/K_{\text{m}} = 1.22 \text{ M}^{-1} \text{ s}^{-1}$  [1]. A coupled peroxidase assay as previously reported for WT GlxA was carried out with the Cu(II)-loaded apo-WT GlxA and the Cu(II)-loaded W288A and W288F variants. For the WT sample activity in line with what has been previously reported was detected [1], but in contrast no guaiacol oxidation product was detected for the W288A and W288F variants despite a myriad of assay conditions sampled (*i.e.* increased variant concentrations, bubbling samples with O<sub>2</sub>, addition of oxidants). This indicates that neither the W288A or W288F variants are capable of producing H<sub>2</sub>O<sub>2</sub> with the *in vitro* substrate glycolaldehyde.

#### *The Cys-Tyr radical is not formed in the Trp288 variants*

EPR spectroscopy has previously been used to detect the 3'-(S-cysteinyl) tyrosine radical in both Gox and GlxA [1, 2, 4]. Addition of either K<sub>3</sub>[Fe(CN)<sub>6</sub>] or K<sub>2</sub>[Ir(Cl)<sub>6</sub>] to the mature WT GlxA or Gox enzymes results in a decrease in the Cu(II) signal and the concomitant appearance of a three component free radical EPR spectrum [1, 28], assigned to a Cys-Tyr radical [2, 4] (Fig. 7). Experimental and computational studies on holo-Gox have shown that the cross-link allows electron delocalization onto the Sγ(Cys), making the Cys-Tyr radical less strongly coupled than a Tyr radical to the Cu(II) centre [29]. As a result of this weaker antiferromagnetic exchange coupling between the radical and Cu(II) site two paramagnetic species may be observed in the EPR spectrum [28]. However, for the W288A and W288F variants, addition of either oxidant does not yield the intense EPR signature seen for WT GlxA (Fig. 7). Instead, a residual signal that is consistent with it being the same as the radical triplet assigned to the 3'-(S-cysteinyl) tyrosine is detected (inset Fig. 7). This indicates that Trp288 is important for stabilising the Cys-Tyr radical. Interestingly, the residual triplet EPR signal is slightly greater in intensity for the W288F variant compared to the W288A

variant (inset Fig. 7). This could mean that a different aromatic residue i.e. Phe in the 288 position can provide some stabilisation, but with an Ala at the 288 position, the yield of the Cys-Tyr radical is next to nothing.

#### *The GlxA Trp288 variants do not complement the glxA null mutant*

From a previous study the *glxA* null mutant is deficient in development and arrested in the vegetative growth phase resulting in a bald phenotype (*i.e.* no aerial mycelium) on R5 agar plates containing 5  $\mu$ M Cu(II) ions [1]. Neither the W288A or the W288F variants are competent to complement the developmental defect in the null mutant (Fig. 8A). In liquid cultures, dense mycelium pellets characterize the morphology of the 1326 strain (Fig. 8B). The *glxA* null mutant grows in liquid with an open mat-type mycelium and does not make the dense pellets (Fig. 8B) [1]. By introducing GlxA expressed from a genome integrated vector under control of its own promoter into the *glxA* null mutant, a phenotype close to that of the parent strain is obtained (Fig. 8B). However, the W288A and W288F variants expressed in the same way do not show the full complementation of the typical *glxA* null mutant phenotype to dense pellets (Fig. 8B). Only the W288F variant produces pellets that to some extent are as seen for the 1326 strain but are nowhere near as dense (Fig. 8B). This effect on mycelium density is confirmed by a sedimentation assay where the 1326 strain requires only minutes to settle completely (Fig. 8C). However, the *glxA* null mutant mycelium does not sediment and remains in suspension after 2 days (Fig. 8C). Upon complementing the mutant with WT GlxA the mycelium settles on a similar time scale as the 1326 strain. However, the *glxA* null mutant strain expressing the W288A variant needs considerable more time for mycelium sedimentation (> 2 days), whereas for the W288F variant an intermediate settling time is observed (Fig. 8C). These data agree with the microscopic view of the morphology (Fig. 8B) and suggest that Trp288 has an important functional role *in vivo*.

## **DISCUSSION**

GlxA is a newly discovered member of the Cu-radical oxidase family that sits alone as the only prokaryotic member of this oxidase family to so far be characterised [1]. Its' known importance in the Cu-dependent development of *S. lividans* has implications in biotechnology for strain development to give better yields of heterologously expressed commercially valuable proteins and enzymes. To this end

understanding the fundamental structural and functional properties of GlxA, including metalation of the Cu site is important. The present study has explored the structure-function role of a Trp residue that acts as a canopy to the Cys-Tyr redox cofactor in GlxA.

In the context of previous studies on the eukaryotic Gox [30-32] the results presented here reveal that Cu is required to initiate the formation of the 3'-(S-cysteinylyl) tyrosine redox cofactor in GlxA. This illustrates that a metal mediated post-translational processing event occurs in a prokaryotic Cu-radical oxidase, an event not previously studied *in vitro*. The role of Cu is particularly apparent from the absence of electron density for a Cys<sup>121</sup>-S $\gamma$ -C $\epsilon$ -Tyr<sup>289</sup> bond in the apo-W288A variant. However, in contrast to Gox, where complete processing to the mature form (a single band on Western blot) has been reported *in vitro* [13], two bands on a Western blot for the W288A and W288F variants and WT GlxA are observed (Fig. 2). This is consistent with the active site heterogeneity observed with the Cu(II)-soaked W288A structure (Fig. 6). The major conformation shows that Cu-binding causes Cys121 and Tyr289 to orientate favourably for initiation of cross-link formation (Fig. 6C). However, the final cross-link does not appear to be formed within the crystal and this may be due to the protein dynamics required for cross-linking being suppressed within the crystal lattice. From band intensities, the WT, W288A and W288F variants are processed to ~ 50 % of the mature enzyme after a 1 h incubation with Cu(II) (Fig. 2). Whereas this ratio of premature/mature forms remain unaltered in the W288A and W288F variants, it is notable that for WT, maturation continues with ~ 75 % processed to the mature form after 72 h (Fig. 2C). Thus, Trp288 appears not to be responsible for incomplete processing of GlxA, but does affect the amount of mature enzyme produced *in vitro* following Cu addition.

A previous study has reported that mycelial extracts taken from liquid grown cultures of *S. lividans* 1326 have a migration pattern on a SDS-PAGE gel consistent with only the presence of the mature GlxA [17]. In a *sco* null mutant, where Sco is an extracytoplasmic Cu metallochaperone [33], premature GlxA is present as evidenced by only the upper band [17]. This implied that Sco was acting to assist (chaperone Cu) in the maturation of GlxA under Cu metallostatic conditions [17]. Interestingly, on supplementing the *sco* mutant with exogenous Cu, two bands with intensities and migration patterns identical to those observed here *in vitro* for the premature and

mature forms of GlxA were identified [17]. Thus, addition of exogenous Cu *in vitro* or *in vivo* is not sufficient to drive complete processing of GlxA to the mature form.

Despite Gox and GlxA sharing the same ligand set, the UV-vis spectrum of the two enzymes in the semi-reduced Cu(II)-(Cys-Tyr) state is distinctly different. It has been reported that Trp290 variants of Gox do not alter the absorbance spectrum [13, 14]. However, replacing Trp288 in GlxA with an aromatic or non-aromatic residue significantly perturbs the Cu(II)-(Cys-Tyr) spectrum compared to WT GlxA, but notably results in essentially the same spectrum for each variant. In fact, these spectra now more closely resemble that of Cu(II)-(Cys-Tyr) Gox [28, 34]. It may therefore be argued that the indole ring orientation of Trp288 in WT GlxA does influence the Cu electronic absorbance spectrum. This is based on the absence of a spectral change with the Gox Trp variants [14] and with a change to a more Gox-like spectrum with the W288A and W288F GlxA variants. By contrast the EPR spectrum of the W288A and W288F variants are much less perturbed compared to WT GlxA (Fig. 4). The EPR spectra can be rationalised as superposition of two Cu(II) EPR signals, Sim1 and Sim2. These two signals have notably different EPR parameters implying differences in ligand geometry. Interestingly, partial composition of the Cu complexes as well as both the signals key EPR parameters exhibit correlations pertaining to the size of the residue at position 288, *i.e.* Sim1 has an increasing  $g$ -factor anisotropy and a decreasing  $A_z^{\text{Cu}}$  value when going from Trp to Phe to Ala (Fig. 4B and Table 2). The exact mechanism of this is not clear but it could be that the different hydrophobic impact of the residue at 288 towards the phenol ring of Tyr289 implements different mobility of the tyrosine (as observed crystallographically) thus producing different ligand field strength onto the Cu(II) ion.

The Cu(II) binding kinetics to the premature form of the W288A and W288F GlxA variants is affected by the type of substitution. Whilst the initial rapid Cu(II) binding phase to form GlxA\*Cu(II) is independent of the type of substitution at position 288, the subsequent rearrangement step ( $k_2$ ) to the final Cu(II) complex is dependent. This difference can be ascribed to steric constraints imposed by the Phe side chain imposing rigidity on the rest of the Cu site. From the X-ray structure of the W288A variant the conformational freedom observed for Cys121 and Tyr289 is due to the absence of the stacking Trp288. Therefore, in the W288F variant it could be envisaged that the Cu site is better formed due to steric constraints imposed by the Phe side chain, *i.e.* sterically preventing the orientation of the phenol ring of Tyr289

observed in the apo-W288A structure (Fig. 6). This suggests that the cross-link formation is coupled to the kinetics of Cu(II) binding. This leads to the several orders of magnitude faster  $k_2$  compared to the W288A variant, where in the latter the formation of the Cys-Tyr cross-link is slower due to the absence of steric constraints imposed by the residue type at position 288. Furthermore, it implies that Cys121 and Tyr289 in the premature WT GlxA are similarly constrained in a favoured orientation for the C $\epsilon$  of Tyr289 to undergo nucleophilic attack by the S $\gamma$  of Cys121 prior to Cu-loading into the site and thus minimising the structural rearrangement required due to the steric restraints imposed by Trp288. This contrasts to the situation in Gox where Trp290 is not adjacent to Tyr272 but on a separate loop structure [3]. This creates a more flexible site in the apo-form of Gox, with the Trp290 being brought into its stacking orientation following cross-link formation [35].

Catalytic efficiency of the Trp290 Gox variants with D-galactose decreases by up to 1000-fold depending on the type of substitution (W290F > W290H > W290G) [14]. This has been attributed in part to the loss of a stabilising interaction between the N $\epsilon$  atom of the indole ring and the bound D-galactose [36, 37] and a decrease in stability (decay rate) of the Cys-Tyr radical [14]. Nevertheless, catalytic activity remains detectable as the variants all retain the capability of forming a Cu(II)-(Cys-Tyr $\bullet$ ) state, which is long enough lived to facilitate turnover [14]. In contrast, catalytic activity of the W288A and W288F GlxA variants with the diose glycolaldehyde is not detectable. This cannot be wholly attributed to only ~ 50 % of the mature form being present in the W288A and W288F variants, as comparable assays with Cu(II) incubated WT GlxA, where ~ 75 % of the mature state is estimated, readily produces H<sub>2</sub>O<sub>2</sub>. These *in vitro* assays corroborate the *in vivo* data suggesting that Trp288 is important for GlxA function. Whilst the chemical composition of the physiological substrate for GlxA is unknown, the removal of the Trp288 effects growth morphology on both solid and liquid medium (Fig. 8). In the case of the latter there is a suggestion that some residual enzymatic activity *in vivo* is present based on the observation that intermediate pellet-like mycelium is formed when expressed in the *glxA* null mutant strain, whereas on solid media, growth is arrested in the vegetative state. Intriguingly, the Phe variant produces denser pellets than the Ala variant (Fig. 8). The *in vitro* EPR data showing the presence of a residual Cu(II)-(Cys-Tyr $\bullet$ ) state for the W288F variant therefore correlates with this *in vivo* difference.

To summarise this work, both *in vitro* and *in vivo* studies have revealed that Trp288 of GlxA clearly acts to stabilise the Cu(II)-(Cys-Tyr•) state sufficiently to enable turnover of a substrate to occur. Furthermore, it seems that the absence of Trp288 in GlxA has a much more detrimental effect than the corresponding Trp290 in Gox. One could expect that if it is simply a  $\pi$ - $\pi$  stacking interaction by Trp288 in GlxA that leads to stabilising the radical, then a Phe may be expected to compensate, if its benzyl ring is stacking in a similar orientation to that of the benzyl ring of the indole. However, results with the W288F variant do not support this and despite the difference in indole ring orientation between Trp290 in Gox and Trp288 in GlxA (Fig. 1B) the electronic and steric effects of a heterocyclic system positioned near the Cys-Tyr cross-link appear critical for radical stability. Furthermore, unlike in Gox the stacking Trp is clearly influencing the electronic absorption spectra of GlxA. Finally, in the context of how enzymes are metalated the findings here and from a previous study [17] reveal that the addition of exogenous Cu *in vitro* or *in vivo* is not sufficient to drive complete processing of GlxA to the mature form. This underscores the important role for metallochaperones, such as Sco, to not only metalate a metalloenzyme with the correct metal but also in the case of GlxA to create the mature active enzyme through a Cu ion driven post-translational event.

#### **ACKNOWLEDGEMENTS**

The award of a University of Essex Silberrad PhD scholarship to AKC is gratefully acknowledged. Dr James Whittaker (Oregon Health and Science University, USA) for the kind gift of GlxA antibodies. Diamond Light Source for access to beamline I03 (East of England Macromolecular Crystallography BAG, MX7461) and use of the JCSG Quality Control Server are acknowledged.

#### **CONFLICTS OF INTEREST**

Authors declare no conflict of interest

#### **AUTHOR CONTRIBUTIONS**

A.K.C. conducted all *in vitro* experiments, prepared all samples and analysed all data. D.A.S. carried out EPR experiments and spectral simulations. M.A.H. supervised the crystallography and structure determination. M.T.W. assisted with stopped-flow

experiments and analysis of the kinetic data. E.V. carried out the *in vivo* work. J.A.R.W designed the study and wrote the manuscript with contributions from all co-authors.

## REFERENCES

- 1 Chaplin, A. K., Petrus, M. L., Mangiameli, G., Hough, M. A., Svistunenko, D. A., Nicholls, P., Claessen, D., Vijgenboom, E. and Worrall, J. A. (2015) GlxA is a new structural member of the radical copper oxidase family and is required for glycan deposition at hyphal tips and morphogenesis of *Streptomyces lividans*. *Biochem J.* **469**, 433-444
- 2 Whittaker, M. M. and Whittaker, J. W. (1990) A tyrosine-derived free radical in apogalactose oxidase. *J Biol Chem.* **265**, 9610-9613
- 3 Ito, N., Phillips, S. E., Stevens, C., Ogel, Z. B., McPherson, M. J., Keen, J. N., Yadav, K. D. and Knowles, P. F. (1991) Novel thioether bond revealed by a 1.7 Å crystal structure of galactose oxidase. *Nature.* **350**, 87-90
- 4 Lee, Y. K., Whittaker, M. M. and Whittaker, J. W. (2008) The electronic structure of the Cys-Tyr free radical in galactose oxidase determined by EPR spectroscopy. *Biochemistry.* **47**, 6637-6649
- 5 Avigad, G., Amaral, D., Asensio, C. and Horecker, B. L. (1962) The D-galactose oxidase of *Polyporus circinatus*. *J Biol Chem.* **237**, 2736-2743
- 6 Whittaker, J. W. (2003) Free radical catalysis by galactose oxidase. *Chem Rev.* **103**, 2347-2363
- 7 Cantarel, B. L., Coutinho, P. M., Rancurel, C., Bernard, T., Lombard, V. and Henrissat, B. (2009) The Carbohydrate-Active EnZymes database (CAZy): an expert resource for Glycogenomics. *Nucleic Acids Res.* **37**, D233-238
- 8 Levasseur, A., Drula, E., Lombard, V., Coutinho, P. M. and Henrissat, B. (2013) Expansion of the enzymatic repertoire of the CAZy database to integrate auxiliary redox enzymes. *Biotechnology for biofuels.* **6**, 41
- 9 Yin, D. T., Urresti, S., Lafond, M., Johnston, E. M., Derikvand, F., Ciano, L., Berrin, J. G., Henrissat, B., Walton, P. H., Davies, G. J. and Brumer, H. (2015) Structure-function characterization reveals new catalytic diversity in the galactose oxidase and glyoxal oxidase family. *Nature communications.* **6**, 10197
- 10 Xu, H., Chater, K. F., Deng, Z. and Tao, M. (2008) A cellulose synthase-like protein involved in hyphal tip growth and morphological differentiation in *Streptomyces*. *J Bacteriol.* **190**, 4971-4978
- 11 van Veluw, G. J., Petrus, M. L., Gubbens, J., de Graaf, R., de Jong, I. P., van Wezel, G. P., Wosten, H. A. and Claessen, D. (2012) Analysis of two distinct mycelial populations in liquid-grown *Streptomyces* cultures using a flow cytometry-based proteomics approach. *Appl Microbiol Biotechnol.* **96**, 1301-1312
- 12 Liman, R., Facey, P. D., van Keulen, G., Dyson, P. J. and Del Sol, R. (2013) A laterally acquired galactose oxidase-like gene is required for aerial development during osmotic stress in *Streptomyces coelicolor*. *PLoS One.* **8**, e54112
- 13 Baron, A. J., Stevens, C., Wilmot, C., Seneviratne, K. D., Blakeley, V., Dooley, D. M., Phillips, S. E., Knowles, P. F. and McPherson, M. J. (1994) Structure and mechanism of galactose oxidase. The free radical site. *J Biol Chem.* **269**, 25095-25105
- 14 Rogers, M. S., Tyler, E. M., Akyumani, N., Kurtis, C. R., Spooner, R. K., Deacon, S. E., Tamber, S., Firbank, S. J., Mahmoud, K., Knowles, P. F., Phillips, S.

- E., McPherson, M. J. and Dooley, D. M. (2007) The stacking tryptophan of galactose oxidase: a second-coordination sphere residue that has profound effects on tyrosyl radical behavior and enzyme catalysis. *Biochemistry*. **46**, 4606-4618
- 15 Kieser, T. B., M.J. Buttner, M.J. Chater, K.F. Hopwood, D.A. (2000) Practical *Streptomyces* Genetics. John Innes Foundation, Norwich, UK
- 16 Deacon, S. E. and McPherson, M. J. (2011) Enhanced expression and purification of fungal galactose oxidase in *Escherichia coli* and use for analysis of a saturation mutagenesis library. *Chembiochem*. **12**, 593-601
- 17 Petrus, M. L., Vijgenboom, E., Chaplin, A. K., Worrall, J. A., van Wezel, G. P. and Claessen, D. (2016) The DyP-type peroxidase DtpA is a Tat-substrate required for GlxA maturation and morphogenesis in *Streptomyces*. *Open biology*. **6**, 150149
- 18 Gasteiger, E., Gattiker, A., Hoogland, C., Ivanyi, I., Appel, R. D. and Bairoch, A. (2003) ExPASy: The proteomics server for in-depth protein knowledge and analysis. *Nucleic Acids Res*. **31**, 3784-3788
- 19 Svistunenko, D. A. and Cooper, C. E. (2004) A new method of identifying the site of tyrosyl radicals in proteins. *Biophysical journal*. **87**, 582-595
- 20 Kabsch, W. (2010) XDS. *Acta Crystallographica Section D-Biological Crystallography*. **66**, 125-132
- 21 Winter, G. (2010) xia2: an expert system for macromolecular crystallography data reduction. *J. Appl. Crystallogr*. **43**, 186-190
- 22 Evans, P. R. and Murshudov, G. N. (2013) How good are my data and what is the resolution? *Acta crystallographica. Section D, Biological crystallography*. **69**, 1204-1214
- 23 Murshudov, G. N., Vagin, A. A. and Dodson, E. J. (1997) Refinement of macromolecular structures by the maximum-likelihood method. *Acta crystallographica. Section D, Biological crystallography*. **53**, 240-255
- 24 Emsley, P. and Cowtan, K. (2004) Coot: model-building tools for molecular graphics. *Acta crystallographica. Section D, Biological crystallography*. **60**, 2126-2132
- 25 Davis, I. W., Leaver-Fay, A., Chen, V. B., Block, J. N., Kapral, G. J., Wang, X., Murray, L. W., Arendall, W. B., 3rd, Snoeyink, J., Richardson, J. S. and Richardson, D. C. (2007) MolProbity: all-atom contacts and structure validation for proteins and nucleic acids. *Nucleic Acids Res*. **35**, W375-383
- 26 Krissinel, E. (2012) Enhanced fold recognition using efficient short fragment clustering. *Journal of Molecular Biochemistry*. **1**, 76-85
- 27 Peisach, J. and Blumberg, W. E. (1974) Structural implications derived from the analysis of electron paramagnetic resonance spectra of natural and artificial copper proteins. *Arch Biochem Biophys*. **165**, 691-708
- 28 Whittaker, M. M. and Whittaker, J. W. (1988) The active site of galactose oxidase. *J Biol Chem*. **263**, 6074-6080
- 29 Rokhsana, D., Howells, A. E., Dooley, D. M. and Szilagy, R. K. (2012) Role of the Tyr-Cys cross-link to the active site properties of galactose oxidase. *Inorg Chem*. **51**, 3513-3524
- 30 Rogers, M. S., Baron, A. J., McPherson, M. J., Knowles, P. F. and Dooley, D. M. (2000) Galactose oxidase pro-sequence cleavage and cofactor assembly are self-processing reactions. *Journal of the American Chemical Society*. **122**, 990-991
- 31 Whittaker, M. M. and Whittaker, J. W. (2003) Cu(I)-dependent biogenesis of the galactose oxidase redox cofactor. *J Biol Chem*. **278**, 22090-22101
- 32 Rogers, M. S., Hurtado-Guerrero, R., Firbank, S. J., Halcrow, M. A., Dooley, D. M., Phillips, S. E., Knowles, P. F. and McPherson, M. J. (2008) Cross-link



formation of the cysteine 228-tyrosine 272 catalytic cofactor of galactose oxidase does not require dioxygen. *Biochemistry*. **47**, 10428-10439

33 Blundell, K. L., Hough, M. A., Vijgenboom, E. and Worrall, J. A. (2014) Structural and mechanistic insights into an extracytoplasmic copper trafficking pathway in *Streptomyces lividans*. *Biochem J*. **459**, 525-538

34 Whittaker, M. M. and Whittaker, J. W. (1993) Ligand interactions with galactose oxidase: mechanistic insights. *Biophysical journal*. **64**, 762-772

35 Firbank, S. J., Rogers, M. S., Wilmot, C. M., Dooley, D. M., Halcrow, M. A., Knowles, P. F., McPherson, M. J. and Phillips, S. E. (2001) Crystal structure of the precursor of galactose oxidase: an unusual self-processing enzyme. *Proc Natl Acad Sci U S A*. **98**, 12932-12937

36 Ito, N., Phillips, S. E., Yadav, K. D. and Knowles, P. F. (1994) Crystal structure of a free radical enzyme, galactose oxidase. *J Mol Biol*. **238**, 794-814

37 Wachter, R. M. and Branchaud, B. P. (1996) Molecular modeling studies on oxidation of hexopyranoses by galactose oxidase. An active site topology apparently designed to catalyze radical reactions, either concerted or stepwise. *Journal of the American Chemical Society*. **118**, 2782-2789

38 Schneider, C. A., Rasband, W. S. and Eliceiri, K. W. (2012) NIH Image to ImageJ: 25 years of image analysis. *Nature methods*. **9**, 671-675

## FIGURE LEGENDS

**Figure 1:** X-ray structures of AA5 mononuclear Cu-radical oxidases. A) Cartoon representations of *Fusarium graminearum* Gox (PDB 1gog) and *Streptomyces lividans* GlxA (PDB 4unm), with the different domains labeled and the Cu ion shown as a turquoise sphere [1, 3]. B) Stick representations of the Cu active sites of Gox and GlxA. The equatorial Cu coordinating H<sub>2</sub>O molecule, which is displaced upon substrate binding, is depicted as a red sphere.

**Figure 2:** Immunoblot analysis of WT GlxA, the C121G, W288A and W288F GlxA variants. SDS-PAGE gels were blotted following detection by GlxA polyclonal antibodies and bar graphs corresponding to the resulting NBT/BCIP stained band intensities from each blot calculated using the ImageJ software [38]. Mature GlxA (3'-(S-cysteinylyl) tyrosine has been formed) = blue and premature GlxA (no formation of the 3'-(S-cysteinylyl) = yellow on the plots, with error bars the standard deviation from three analysis. Incubation periods with Cu are indicated in hours and molecular weight markers reported in kDa.

**Figure 3:** UV-visible spectroscopy of Cu(II)-binding to the GlxA W288A and W288F variants at pH 8 and 20 °C. A) Absorbance changes associated with the W288F variant upon titration of a Cu(II) solution to the as purified enzyme. Inset, the

change in absorbance at 480 nm plotted as a function of the [Cu(II)]/[W288F] ratio with the solid lines through the data points intersecting at a stoichiometry of  $\sim 1$ . B) Total absorbance change associated with the W288A variant upon the stoichiometric addition of 1 equivalent of Cu(II). Inset, the change in absorbance at 480 nm monitored over time with data points fitted to a single exponential function to yield a rate constant. C) Comparison of the UV-vis spectrum of Cu(II)-Cys-Tyr WT and the W288A and W288F variants.

**Figure 4:** EPR spectroscopy of WT and the W288A and W288F GlxA variants. A) Experimental EPR spectra are shown in blue, with their approximations (in red) being linear combinations of simulated EPR signals Sim1 and Sim2, shown in green and purple, respectively. The amplitudes of the simulated spectra are normalised to equal second integrals, allowing an estimate (in %) of the contribution of the two types of Cu(II) spectra in each protein. Each simulated spectrum has three principal g-values indicated (specified in Table 2), the values are also presented on a common for all variants g-value axis in (B). The *insets* show the hyperfine splitting in the zoomed in  $g_{\perp}$  region of the experimental and the linear combinations of the simulated spectra. Spectra were measured at 40 K at a microwave power of 3.18 mW, modulation frequency of 100 kHz, modulation amplitude of 5 G, time constant of 82 ms and a scan rate of 22.6 G/s. B) Visualisation of the principal g-values of the simulated spectra Sim1 and Sim2 for GlxA and the W288A and W288F variants (see values in Table 1). Note that  $g_z$  values were measured directly from the spectra while  $g_x$  and  $g_y$  were found from the optimization (spectra simulation) procedure.

**Figure 5:** Stopped-flow kinetics of Cu(II) binding to the W288A and W288F GlxA variants at pH 8 and 25 °C. A) Pseudo-first order rate constants ( $k_{\text{obs}}$ ) obtained at 480 nm from fitting time courses (inset; full time course 0-200 s and the first 25 s to illustrate the lag phase) to a single exponential function (red line) generated on mixing the W288F variant with various [Cu(II)]. The black solid line indicates a fit to the data using Equation 1 (see main text). Pseudo-first order rate constants ( $k_{\text{obs}}$ ) obtained at 280 nm for B) the W288F variant and C) the W288A variant on mixing with various [Cu(II)] obtained from fitting the time courses (inset) to a single exponential

function (red line). The straight solid lines represent a linear fit to the data to obtain a second order rate constant.

**Figure 6:** X-ray crystal structures of the W288A GlxA variant. A)  $2F_o-F_c$  electron density map contoured at  $1\sigma$  of the Cu active site in the apo-W288A GlxA variant. Amino acids discussed in the main text are labelled. B) Superposition of the Cu active site in WT (green) [1], apo-W288A (red) and Cu-W288A (blue) GlxA. C)  $2F_o-F_c$  electron density map contoured at  $1\sigma$  of the Cu active site in the Cu-W288A GlxA variant. The major and minor conformations for Cys121, Phe261 and Tyr289 have been labelled a and b, respectively. Bonding interactions (polar in A or coordinate in C) are shown as dashed red lines.

**Figure 7:** Radical EPR spectra of WT GlxA and the W288A and W288F variants. Spectra were measured at 40 K at the microwave power  $P_{MW} = 3.18$  mW, microwave frequency  $\nu_{MW} = 9.465$  GHz; modulation frequency  $\nu_M = 100$  kHz; modulation amplitude  $A_M = 5$  G; scan rate  $\nu = 22.4$  G/s; time constant  $\tau = 81.92$  ms; conversion time, at a 2048 data point scan range,  $t_{conv} = 81.92$  ms. The free radical areas of the spectra are shown in detail in the *inset*.

**Figure 8:** Morphology of *S. lividans* 1326, the *glxA* null mutant and the null mutant complemented with GlxA (WT) and the W288A and W288F variants on solid and in liquid medium. A) Respective strains (600 spores/spot) plated on R5 medium supplemented with  $5 \mu\text{M}$  Cu(II) ions. Pictures were taken after 4 days with a digital camera. Production of aerial hyphae and spores results in the mycelium changing colour to white/grey. For development blocked in the vegetative growth phase (no aerial structures produced) the mycelium remains yellow/red, with the red colour arising from the production of the pigment undecylprodigiosin. B) TSB liquid medium supplemented with 10 % sucrose (TSBS) and  $5 \mu\text{M}$  Cu(II) ions inoculated with spores of the respective strain. After 18 h, mycelium morphology was recorded by light microscopy. All microscope images are recorded with the same magnification, indicated by the bar in the top right corner ( $100 \mu\text{m}$ ). C) Sedimentation assay in which cultures were transferred to tubes and left standing at room temperature.

**Scheme 1**

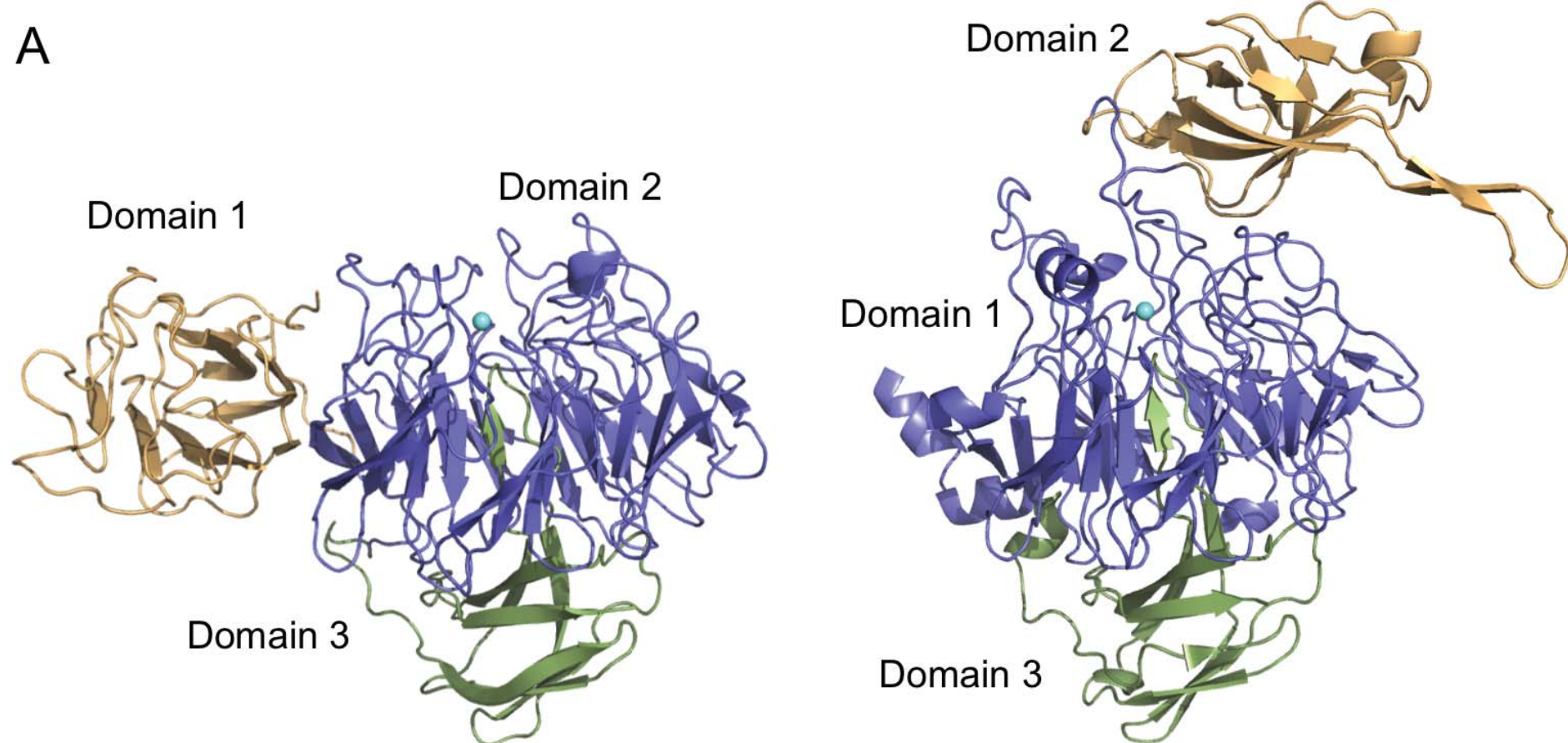
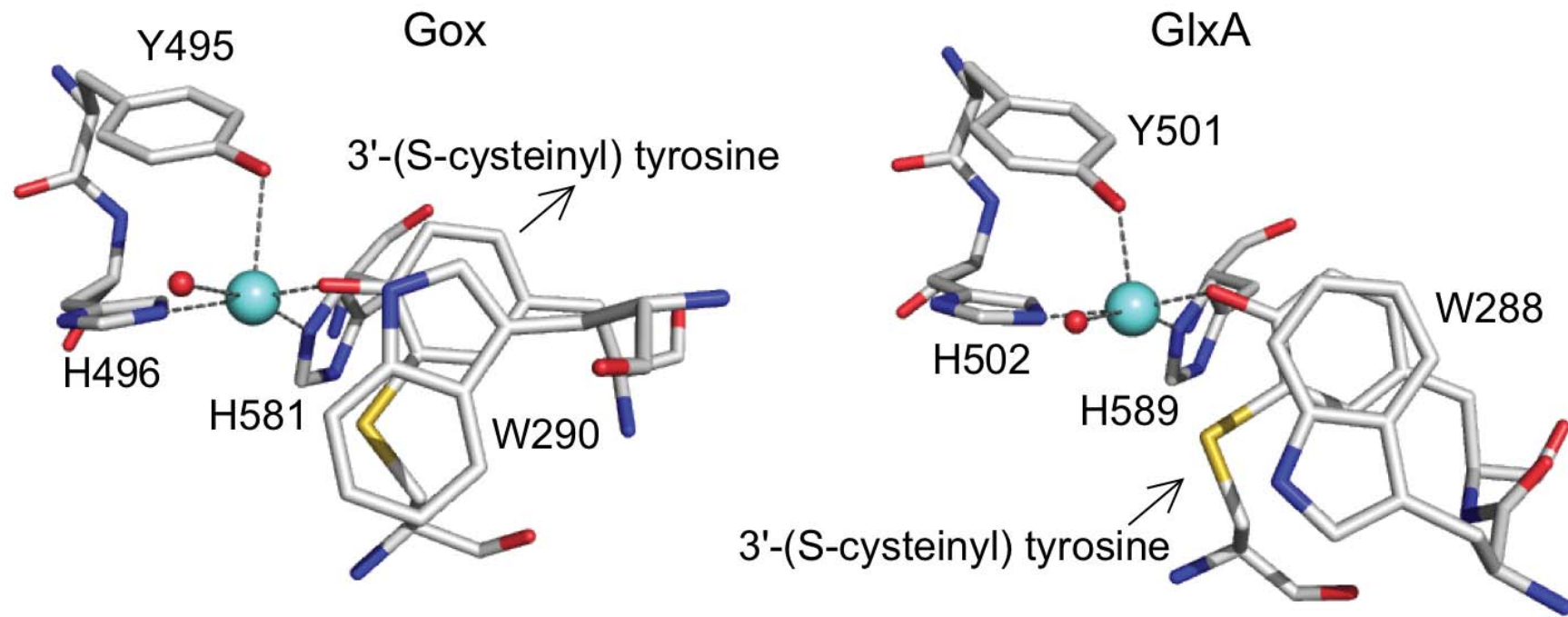


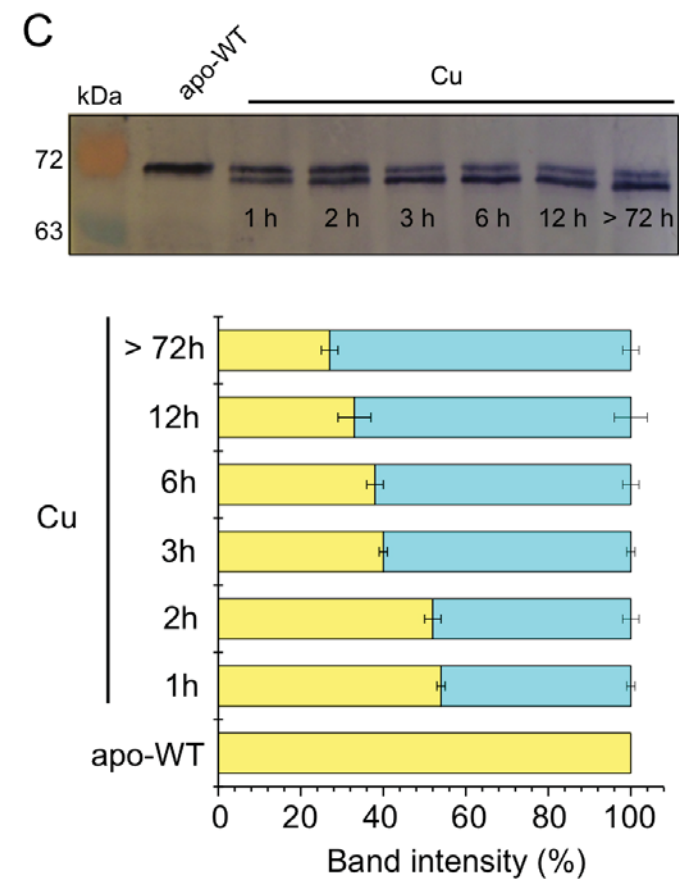
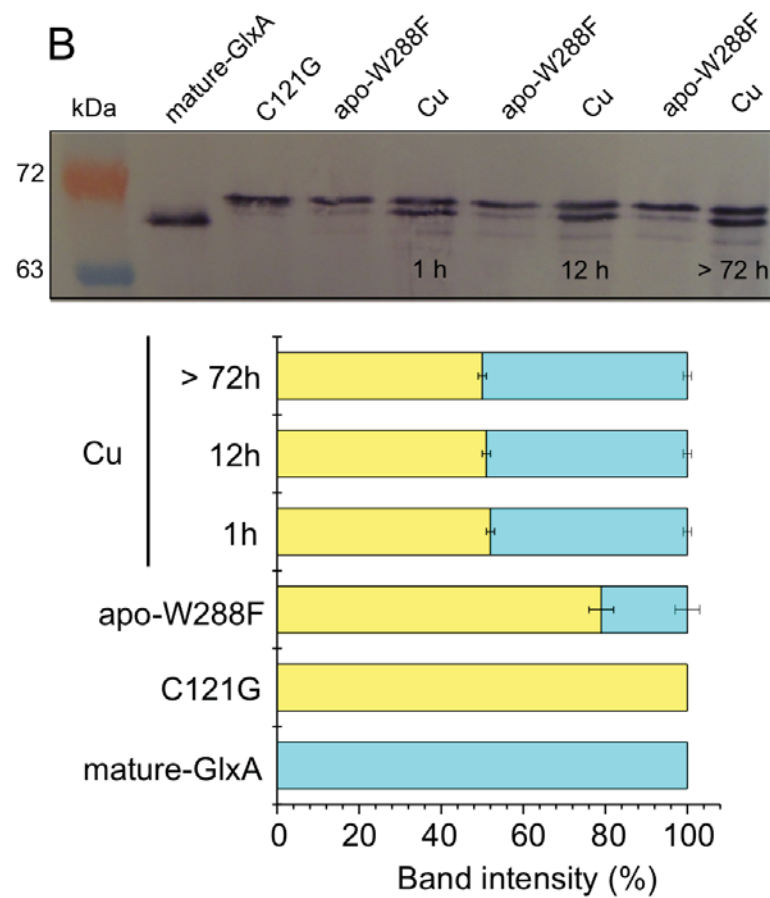
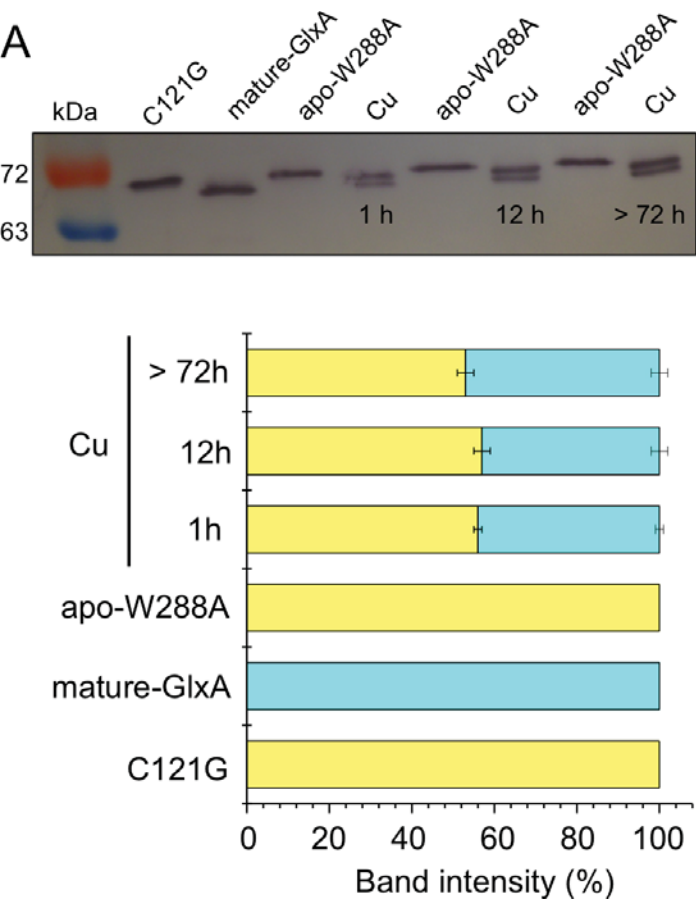
**Table 1:** Crystallographic data processing and refinement statistics for the W288A GlxA variant. Values in parentheses refer to the outermost resolution shells (1.95-1.92 Å and 1.52-1.49 Å for the apo and Cu structures, respectively).

	Apo-W288A	Cu-W288A
Wavelength (Å)	1.00	1.00
Resolution (Å)	1.92	1.49
Space group	P2 <sub>1</sub>	P2 <sub>1</sub> 2 <sub>1</sub> 2 <sub>1</sub>
Unit cell	a = 50.5, b = 126.3, c = 106.9 Å, β = 91.2 °	a = 70.5, b = 80.9, c = 140.3 Å
Unique reflections	99551	130534
Completeness (%)	97.6 (94.9)	99.5 (99.5)
R <sub>merge</sub>	0.073 (0.865)	0.090 (0.754)
Mn (I/SD)	11.7 (2.0)	7.6 (2.0)
CC <sub>1/2</sub>	0.997 (0.768)	0.991 (0.616)
Redundancy	3.6 (3.6)	3.7 (3.8)
Wilson B-factor (Å <sup>2</sup> )	20.5	10.4
R <sub>cryst</sub>	0.182	0.163
R <sub>free</sub>	0.224	0.181
RMS dev. Bond lengths (Å)	0.015	0.013
RMS dev. Bond angles (°)	1.74	1.66
Ramachandran favoured (%)	96.3	97.1
PDB accession code	5LQI	5LXZ

**Table 2:** EPR simulation parameters of WT GlxA and the W288A and W288F variants used to simulate spectra Sim1 and Sim2 in Fig. 4.

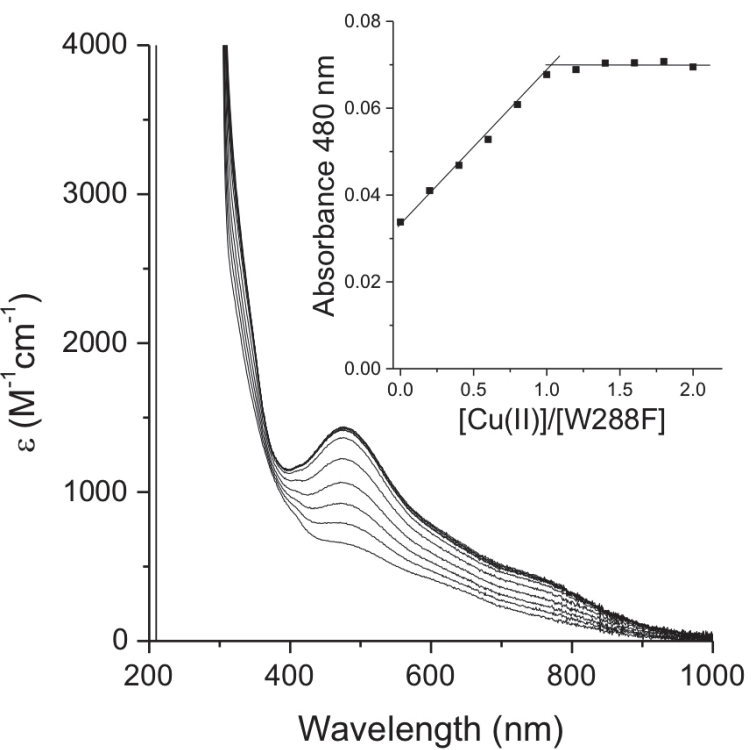
		g	A <sup>Cu</sup> (G)	A <sup>N</sup> (G)	ΔH (G)	
WT	Sim1	x	2.037	17.2	14	12
		y	2.083	17.2	14	12
		z	2.270	172	14	25
	Sim2	x	2.033	20.2	14	12
		y	2.057	20.2	14	10
		z	2.182	202	14	19
W288F	Sim1	x	2.027	15.5	14	12
		y	2.073	15.5	14	12
		z	2.280	155	14	30
	Sim2	x	2.020	20.2	14	12
		y	2.060	20.2	14	11
		z	2.182	202	14	21
W288A	Sim1	x	2.029	13.7	14	12
		y	2.069	13.7	14	12
		z	2.283	137	14	26
	Sim2	x	2.054	21.5	14	12
		y	2.064	21.5	14	12
		z	2.178	215	14	19

**A****B**

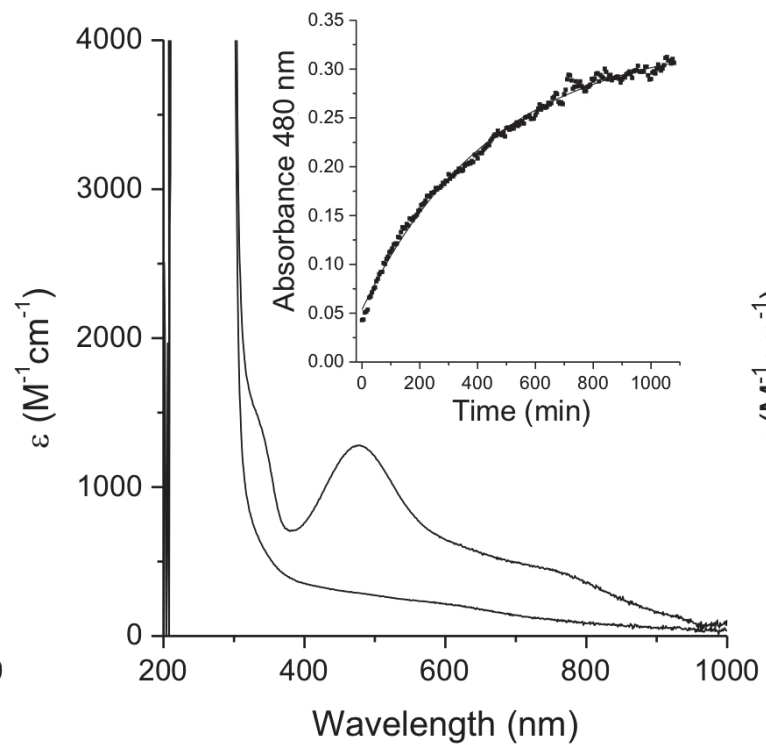




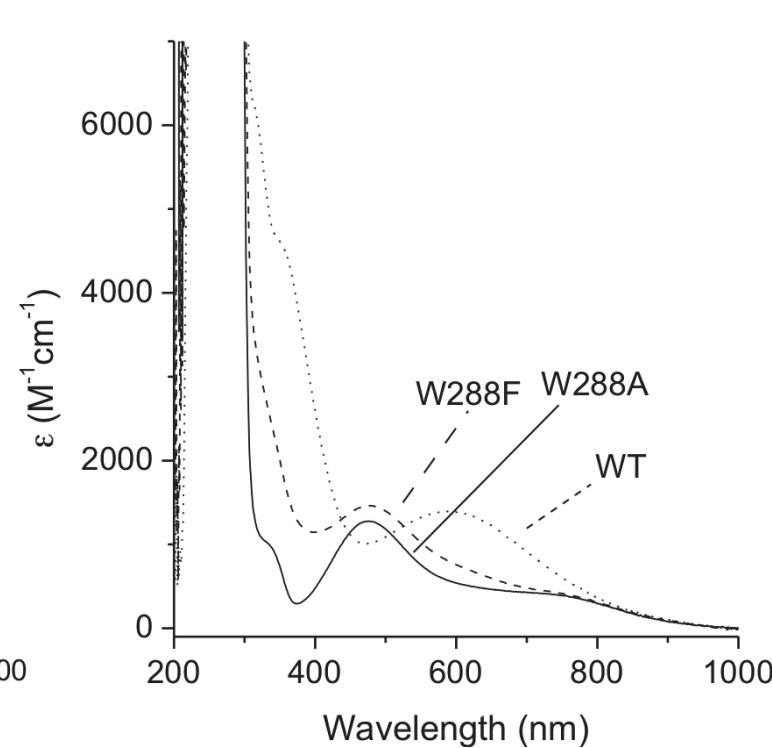
A

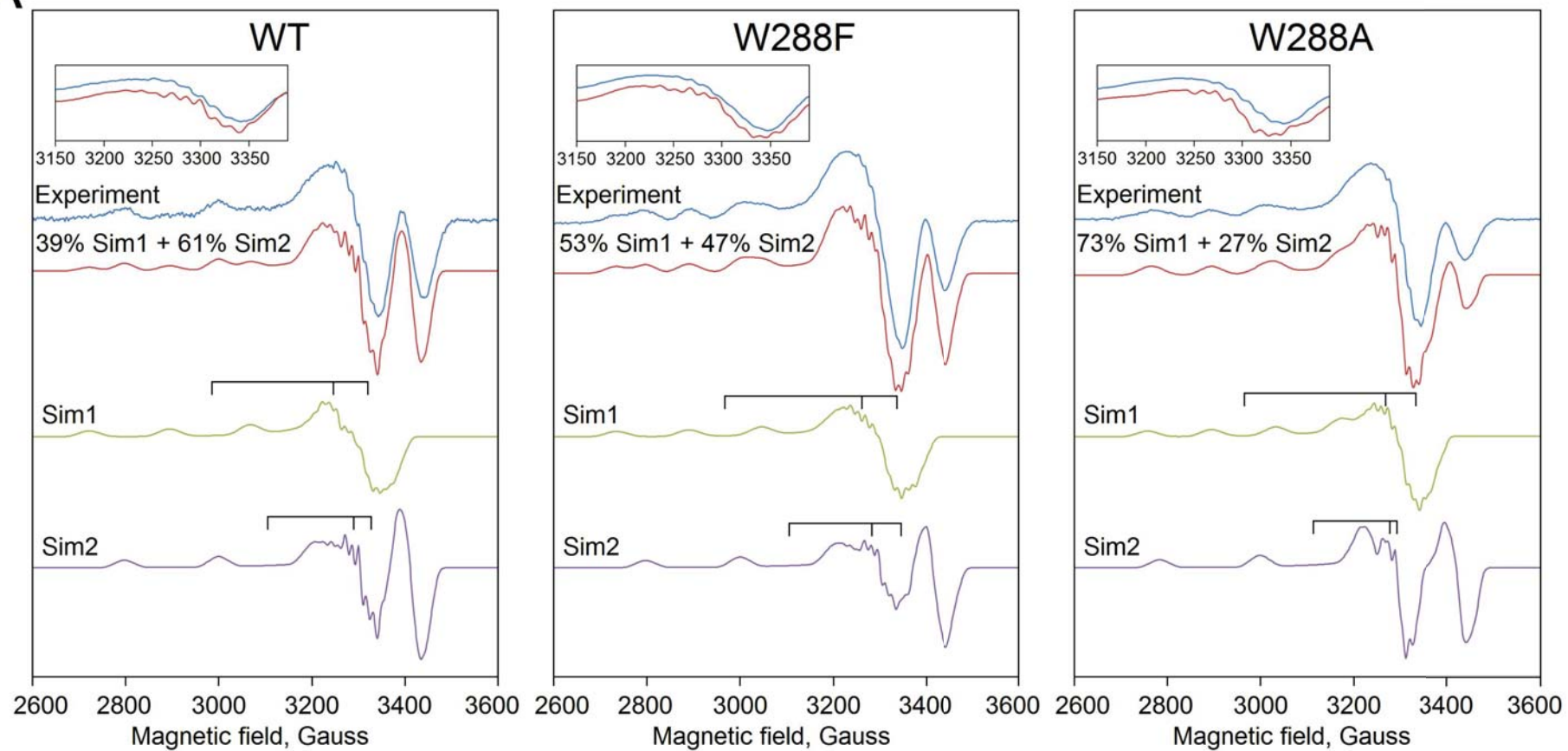
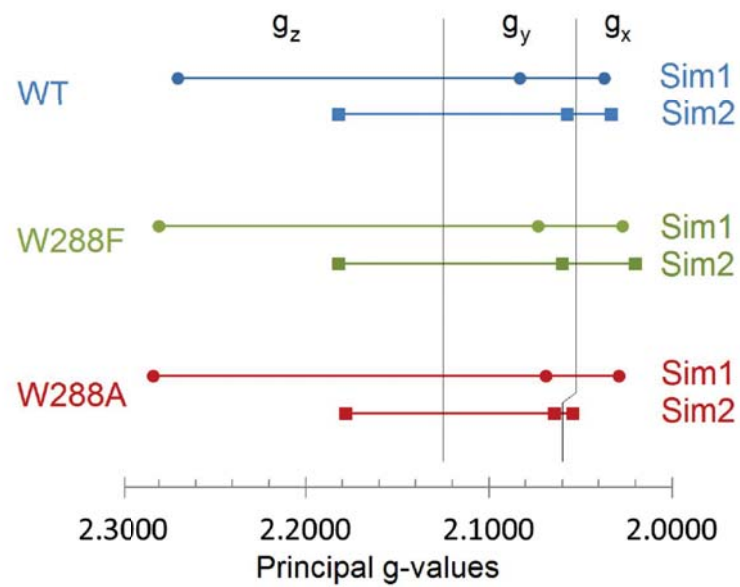


B

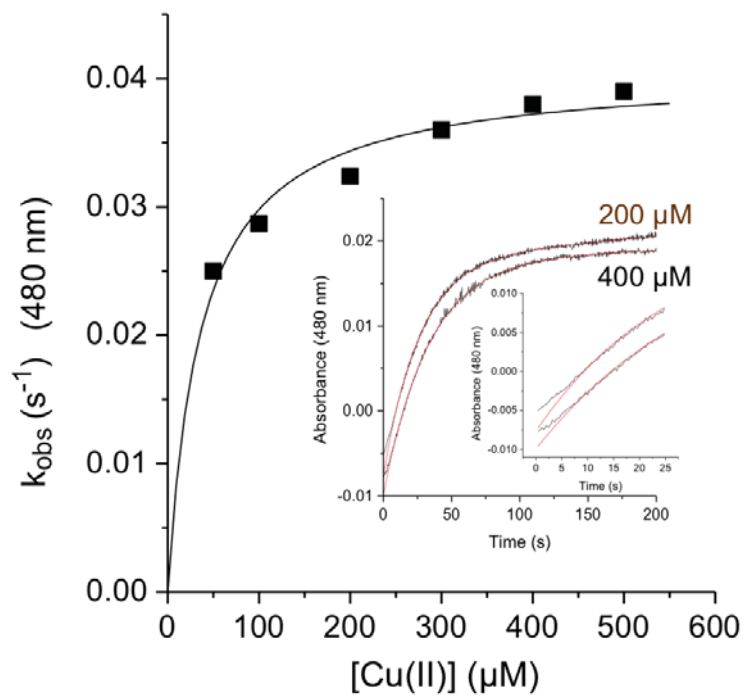


C

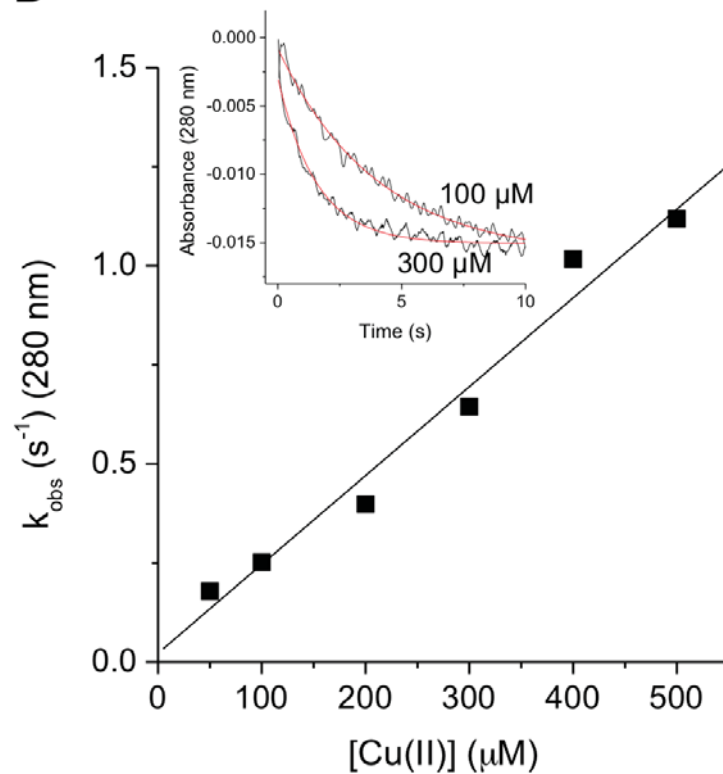


**A****B**

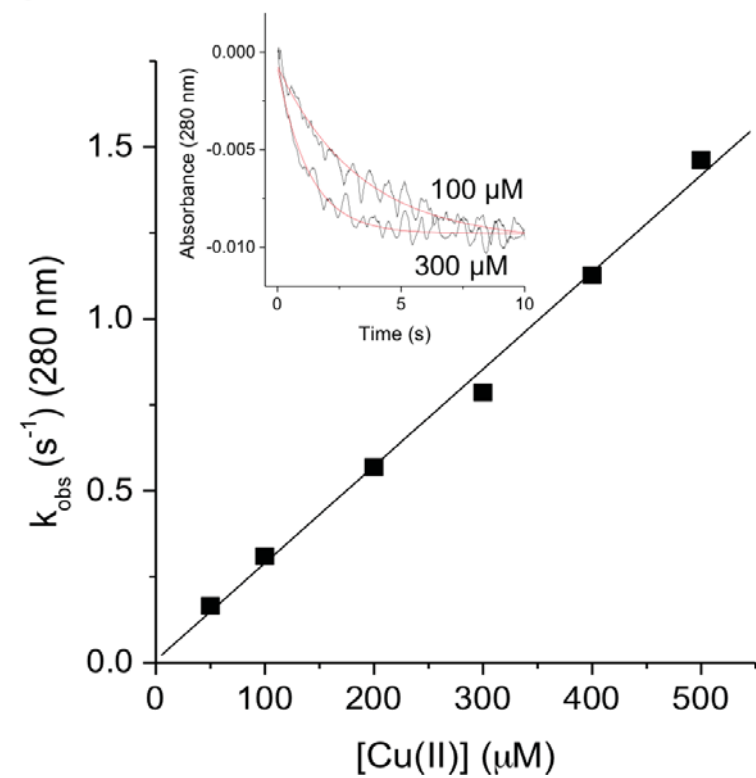
A



B

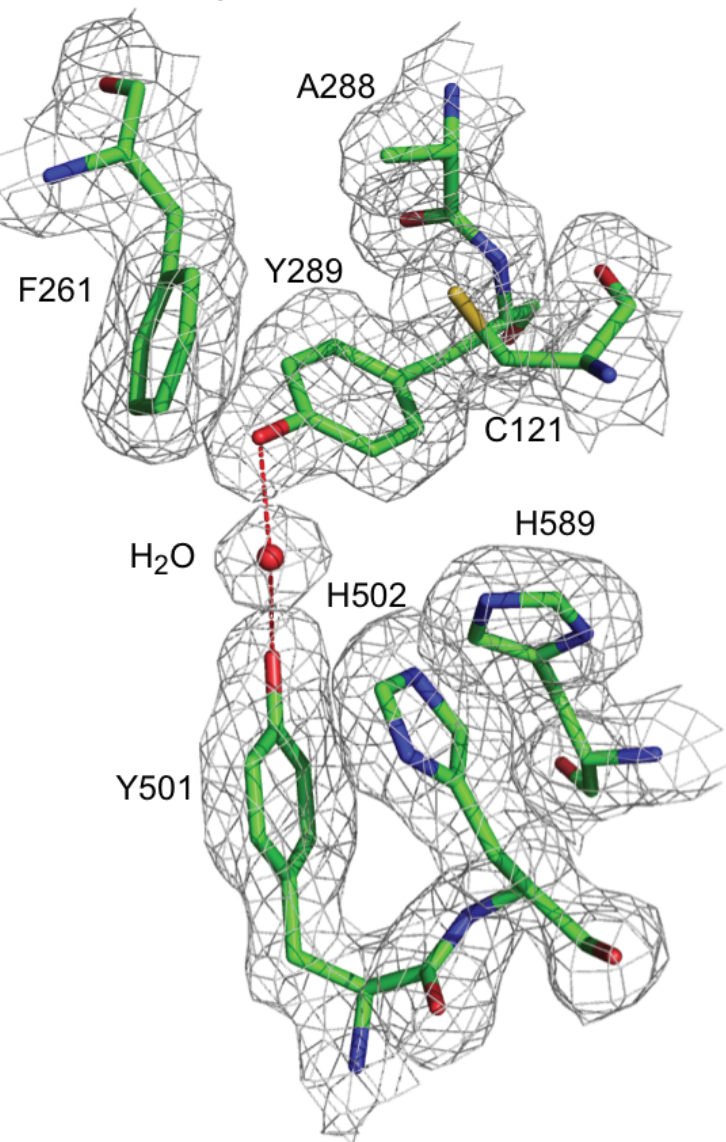


C

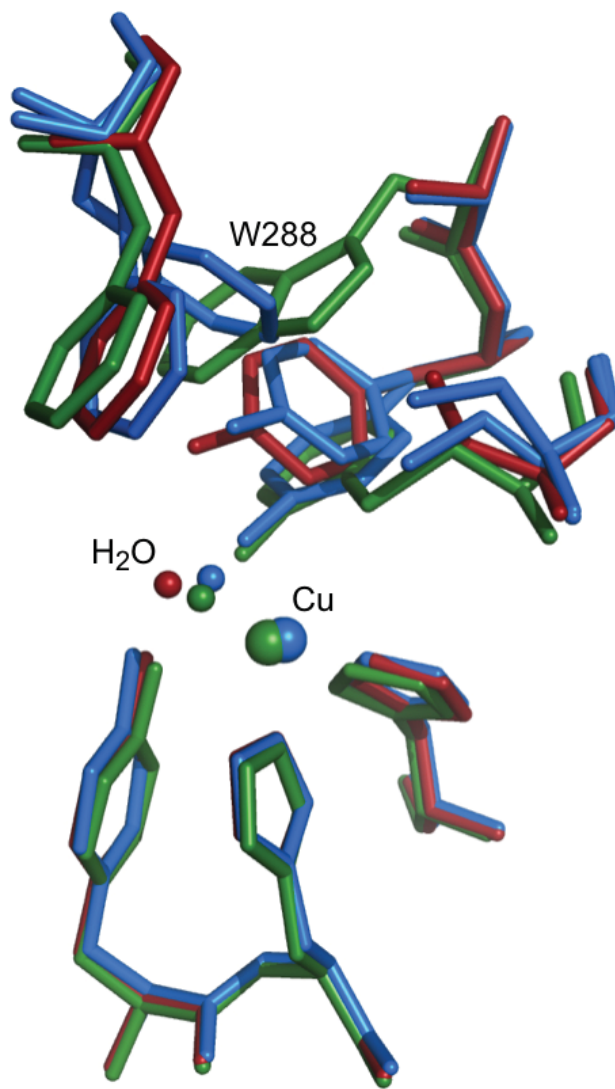


A

apo-W288A



B



C

Cu-W288A

